X-ray holography: theory and experiment

2001 J. Phys.: Condens. Matter 13 10613

(http://iopscience.iop.org/0953-8984/13/47/306)

INSTITUTE OF PHYSICS PUBLISHING JOURNAL OF PHYSICS: CONDENSED MATTER

J. Phys.: Condens. Matter **13** (2001) 10613–10623 PII: S0953-8984(01)26186-4

X-ray holography: theory and experiment

M Tegze and G Faigel

Research Institute for Solid State Physics and Optics, H-1525 Budapest, PO Box 49, Hungary

Received 27 June 2001
Published 9 November 2001
Online at stacks.iop.org/JPhysCM/13/10613

Abstract

A detailed description of x-ray fluorescent holography is given using the formalism of classical electrodynamics. Effects of the wavefront curvature are calculated. It is shown that neglecting these effects might cause large errors especially in the forward direction. The model calculation is compared with experimental data. It is shown that for the model system of NiO the experiment agrees well with theoretical images.

1. Introduction

In the last ten years holographic techniques were developed for structural studies on the atomic scale. First methods using electrons as hologram-forming waves [1, 2], and later x-ray based techniques were realized [3, 4]. Electrons are not ideal for holographic imaging, because of their strong interaction with matter, and the large phase shifts on scattering. These factors lead to distortion in the hologram. To compensate for this, corrections in the evaluation process were introduced. Several works related to electron-holographic evaluation were published in the literature [5]. The situation is somewhat different in the case of x-ray holography. X-ray photons interact with matter much more weakly than electrons, so they produce almost ideal holograms. Therefore in a first approximation the simple Helmholtz–Kirchoff integral transformation [6] gives a reasonable reconstruction. Further, model calculations based on single scattering theory and plane wave approximations describe quite well the formation of x-ray holograms. Lately, the experimental techniques of x-ray holography have been improved to a level which allows the collection of very high quality data. The comparison of model calculations and experimental data shows that at this precision there are differences. This calls for more refined theoretical approaches. In the last few years several papers in this field have been published [7–10]. Calculations based on classical and quantum electrodynamics were both presented. A correct description of all processes and features is given by the quantum theory. However, in this case the derivation of practically useable formulas is very cumbersome. Further these works show that quantum corrections are small. Therefore the use of classical electrodynamics is justified. Even in the classical description different approximations are used. Beside the simplest single scattering plane wave approximation, approaches taking in to account the curvature of the wavefront can be used. Adams and co-workers published a

work of this type [8]. In their paper near field effects were analysed. However, only part of the distortions caused by the curvature of the wavefront was described. Looking at the problem of holography with inside reference points we find three characteristic distances: the wavelength, the interatomic distances and the size of the electron cloud. The ratio between these determines the size of the error caused by neglecting the curvature of the wavefront. In Adams' calculations the wavelength was compared to the interatomic distances. However, the size of the electron cloud was not properly handled. The scattering of electrons was described by the usual atomic scattering factors based on plane waves. In this paper we show that taking into account the size of the electron cloud gives at least as large correction as that coming from the near field effect.

In the following part of the paper we give the basic formulation of holography using the formalism of classical electrodynamics. The normal and inverse holography are discussed separately. However, those parts which are the same or can be described analogously for the inverse case are not repeated. In the next part, the calculations are compared with experimental results on the model system of NiO. In the last section we conclude and discuss future possibilities.

2. Results and discussion

Atomic resolution in holographic imaging can be obtained by using short wavelength hard x-rays and reference points within the sample. Two ways of doing these experiments have been suggested and demonstrated [3, 4, 11]. In the first one selected atoms are excited by an external x-ray source. In the de-excitation of the electronic system fluorescent photons are emitted. These are used to form the hologram. They can reach the detecting surface directly (reference wave) or they can be scattered by the atoms neighbouring the fluorescing one (object wave). These two waves interfere and form the hologram of the environment of the centre atom. This method is called inside source or normal x-ray fluorescent holography.

The other possibility is to form the hologram by the incident beam. In this case the incident x-ray photons can reach the selected atom in the sample directly (reference wave) or by scattering on the neighbours of the centre atom (object wave). The superposition of these two waves at the centre atom determines the excitation amplitude of this atom. After excitation it emits a fluorescent photon. Changing the direction of the incident beam compared to the sample changes the amplitude of the interference field at the centre atom. This reflects in the fluorescent radiation. Detecting these photons as a function of the incident beam direction results in a hologram of the environment of the centre atom. This method is called inside detector or inverse fluorescent x-ray holography, referring to the fact that this experiment is in a reciprocity relation to the normal one.

Let us start with the formulation of normal x-ray fluorescent holography.

In this case an atom inside the sample is excited by an external x-ray source. The excited atom emits fluorescent x-radiation during de-excitation. This radiation is a dipole radiation, and can be described using classical electrodynamics [12]. Placing the fluorescent atom at the origin, the electric field of the emitted radiation at point $\boldsymbol{r}$ is

$$\boldsymbol{E}(\boldsymbol{r}) = k^2(\boldsymbol{n}' \times \boldsymbol{p} \times \boldsymbol{n}')\frac{\mathrm{e}^{\mathrm{i}kr}}{r} + [3\boldsymbol{n}'(\boldsymbol{n}' \cdot \boldsymbol{p}) - \boldsymbol{p}]\left(\frac{1}{r^2} - \frac{\mathrm{i}k}{r}\right)\frac{\mathrm{e}^{\mathrm{i}kr}}{r} \tag{1}$$

where $\boldsymbol{p}$ is the dipole moment of the atom, $\boldsymbol{n}' = \boldsymbol{r}/r$ is the unit vector in the direction of $\boldsymbol{r}$ and $k = 2\pi/\lambda$ is the wavenumber of the fluorescent radiation with wavelength λ. An electron placed at point $\boldsymbol{r}$ in the field of the fluorescent radiation scatters this radiation. The amplitude

of the scattered wave in the far field at point $\boldsymbol{R}$ [12] is given by

$$\boldsymbol{E}_r(\boldsymbol{R}) = r_e \boldsymbol{n} \times [\boldsymbol{n} \times \boldsymbol{E}(\boldsymbol{r})] \frac{\mathrm{e}^{\mathrm{i}k|\boldsymbol{R}-\boldsymbol{r}|}}{|\boldsymbol{R}-\boldsymbol{r}|}. \tag{2}$$

Here $\boldsymbol{n} = (\boldsymbol{R}-\boldsymbol{r})/|\boldsymbol{R}-\boldsymbol{r}|$. Inserting (1) yields

$$\boldsymbol{E}_r(\boldsymbol{R}) = r_e k^2 \frac{\mathrm{e}^{\mathrm{i}k|\boldsymbol{R}-\boldsymbol{r}|}}{|\boldsymbol{R}-\boldsymbol{r}|} \frac{\mathrm{e}^{\mathrm{i}kr}}{r} \boldsymbol{F}(\boldsymbol{k}, \boldsymbol{r}, \boldsymbol{p}) \tag{3}$$

where

$$\boldsymbol{F}(\boldsymbol{k}, \boldsymbol{r}, \boldsymbol{p}) = \boldsymbol{n} \times [\boldsymbol{n} \times (\boldsymbol{n}' \times \boldsymbol{p} \times \boldsymbol{n}')] + \boldsymbol{n} \times \{\boldsymbol{n} \times [3\boldsymbol{n}'(\boldsymbol{n}' \cdot \boldsymbol{p}) - \boldsymbol{p}]\} \left(\frac{1}{r^2 k^2} - \frac{\mathrm{i}}{rk} \right) \tag{4}$$

contains all vector products related to the polarization and radiation directions. Since $R \gg r$, the wavevector in the far field can be written as $\boldsymbol{k} = k\boldsymbol{n} \approx \boldsymbol{R}/R$. Using the approximation $|\boldsymbol{R}-\boldsymbol{r}| \approx R - \boldsymbol{n}\cdot\boldsymbol{r} = R - (\boldsymbol{k}\cdot\boldsymbol{r})/k$ in the first exponential in (3) and $|\boldsymbol{R}-\boldsymbol{r}| \approx R$ in the denominator,

$$\boldsymbol{E}_r(\boldsymbol{R}) = r_e k^2 \frac{\mathrm{e}^{\mathrm{i}kR}}{R} \frac{\mathrm{e}^{\mathrm{i}(kr - \boldsymbol{k}\cdot\boldsymbol{r})}}{r} \boldsymbol{F}(\boldsymbol{k}, \boldsymbol{r}, \boldsymbol{p}). \tag{5}$$

Equation (5) gives the object wave contribution of a single electron to the hologram. Up to now we have followed the treatment by Adams and co-workers [8]. At this point, they introduce the effect of the atomic charge density distribution by replacing r_e by the atomic scattering form factors. However, this approximation is not fully justified, since the atomic form factors are calculated for the scattering of plane waves, and for the nearest neighbour atoms the curvature of the wavefront can be considerably large to influence the scattering amplitude. As we will see later, there are cases when this effect can be larger than the near field effects caused by the second term in equation (1). Instead of multiplying equation (5) by the scattering factors, we start from the electron density in the solid:

$$\rho(\boldsymbol{r}) = \sum_j \rho_j(\boldsymbol{r} - \boldsymbol{r}_j) \tag{6}$$

where ρ_j is the electron density of an atom at position r_j. In the summation over the atoms in the crystal the fluorescent atom at the origin is excluded. If we place a detector in the far field at $\boldsymbol{R}$, the amplitude at the detector is given by the sum of the direct radiation from the fluorescent emitter (reference wave) and the radiation scattered by the charge density of the crystal (object wave):

$$\boldsymbol{E}_D(\boldsymbol{R}) = \boldsymbol{E}(\boldsymbol{R}) + \int \rho(\boldsymbol{r}) \boldsymbol{E}_r(\boldsymbol{R})\, \mathrm{d}^3 r. \tag{7}$$

Since $Rk \ll 1$, according to equation (1) the radiation of the fluorescent atom at $\boldsymbol{R}$ is

$$\boldsymbol{E}(\boldsymbol{R}) = k^2 (\boldsymbol{n} \times \boldsymbol{p} \times \boldsymbol{n}) \frac{\mathrm{e}^{\mathrm{i}kR}}{R}. \tag{8}$$

Inserting equations (5) and (6) into (7), the amplitude at the detector is

$$\boldsymbol{E}_D(\boldsymbol{R}) = k^2 \frac{\mathrm{e}^{\mathrm{i}kR}}{R} \left[(\boldsymbol{n} \times \boldsymbol{p} \times \boldsymbol{n}) + r_e \sum_j \int \rho_j(\boldsymbol{r} - \boldsymbol{r}_j) \frac{\mathrm{e}^{\mathrm{i}(kr - \boldsymbol{k}\cdot\boldsymbol{r})}}{r} \boldsymbol{F}(\boldsymbol{k}, \boldsymbol{r}, \boldsymbol{p})\, \mathrm{d}^3 r \right]. \tag{9}$$

The charge density of an atom is located around its position r_j. Therefore the contribution of a single atom with atomic number Z_j to the object wave amplitude is in the order of $Z_j r_e / r_j$ relative to the reference wave. Since the classical electron radius is $r_e = 2.8 \times 10^{-5}$ Å and the nearest neighbour distances in a crystal are in the ångström range, for an element with a medium atomic number $Z_j r_e / r_j \approx 10^{-4}$–$10^{-3}$. The intensity recorded by the detector is the

sum of three terms: the intensity of the reference wave, the interference between the reference and the object wave and the intensity of the object wave. For small clusters, the last term is negligible. For macroscopic crystals, in directions satisfying the Bragg condition there is constructive interference, which leads to the appearance of Kossel lines [13]. It can be shown that the atoms near to the source atom give no significant contribution to these lines. On the other hand, the effect of these sharp lines can be avoided by applying a low pass spatial filter to the hologram [14, 15]. Since the third term in the expression of the intensity changes only the fine structure of these lines, omitting this term have no effect on the low frequency part of the hologram. Thus the intensity at the detector,

$$|\boldsymbol{E}_D(\boldsymbol{R})|^2 \approx \frac{k^4}{R^2}\left[|\boldsymbol{n}\times\boldsymbol{p}\times\boldsymbol{n}|^2 + 2r_e\sum_j \mathrm{Re}\int \rho_j(\boldsymbol{r}-\boldsymbol{r}_j) \times\frac{\mathrm{e}^{\mathrm{i}(kr-\boldsymbol{k}\cdot\boldsymbol{r})}}{r}(\boldsymbol{n}\times\boldsymbol{p}\times\boldsymbol{n})\cdot\boldsymbol{F}(\boldsymbol{k},\boldsymbol{r},\boldsymbol{p})\,\mathrm{d}^3r\right]. \tag{10}$$

The multiple vector products in this equation can be expressed in terms of scalar products:

$$|\boldsymbol{n}\times\boldsymbol{p}\times\boldsymbol{n}|^2 = p^2-(\boldsymbol{p}\cdot\boldsymbol{n})^2 \tag{11}$$

$$(\boldsymbol{n}\times\boldsymbol{p}\times\boldsymbol{n})\cdot\boldsymbol{F}(\boldsymbol{k},\boldsymbol{r},\boldsymbol{p}) = -[p^2-(\boldsymbol{p}\cdot\boldsymbol{n})^2-(\boldsymbol{p}\cdot\boldsymbol{n}')^2+(\boldsymbol{p}\cdot\boldsymbol{n})(\boldsymbol{p}\cdot\boldsymbol{n}')(\boldsymbol{n}\cdot\boldsymbol{n}')] +[p^2-(\boldsymbol{p}\cdot\boldsymbol{n})^2-3(\boldsymbol{p}\cdot\boldsymbol{n}')^2+3(\boldsymbol{p}\cdot\boldsymbol{n})(\boldsymbol{p}\cdot\boldsymbol{n}')(\boldsymbol{n}\cdot\boldsymbol{n}')]\left(\frac{1}{r^2k^2}-\frac{\mathrm{i}}{rk}\right). \tag{12}$$

The fluorescent radiation of an atom is unpolarized, i.e. the dipole moment vector $\boldsymbol{p}$ can take any direction. Averaging the vector expressions in (11) and (12):

$$\langle(\boldsymbol{p}\cdot\boldsymbol{n})^2\rangle = \langle(\boldsymbol{p}\cdot\boldsymbol{n}')^2\rangle = \tfrac{1}{3}p^2 \tag{13}$$

and

$$\langle(\boldsymbol{p}\cdot\boldsymbol{n})(\boldsymbol{p}\cdot\boldsymbol{n}')\rangle = \tfrac{1}{3}p^2\cos\theta \tag{14}$$

with $\cos\theta = \boldsymbol{n}\cdot\boldsymbol{n}'$, where θ is the scattering angle between vectors $\boldsymbol{r}$ and $\boldsymbol{k}$. Averaging equation (10) for the direction of $\boldsymbol{p}$, and inserting equations (11)–(14), the intensity measured by the detector

$$\langle|\boldsymbol{E}_D(\boldsymbol{R})|^2\rangle = \frac{2k^4p^2}{3R^2}\left[1-2r_e\sum_j \mathrm{Re}\int \rho_j(\boldsymbol{r}-\boldsymbol{r}_j) \times\frac{\mathrm{e}^{\mathrm{i}(kr-\boldsymbol{k}\cdot\boldsymbol{r})}}{r}\left\{P_0(\theta)+[2-3P_0(\theta)]\left(\frac{1}{r^2k^2}-\frac{\mathrm{i}}{rk}\right)\right\}\mathrm{d}^3r\right] \tag{15}$$

where $P_0(\theta) = (1+\cos^2\theta)/2$ is the usual polarization factor for scattering of unpolarized x-rays. We can write equation (15) in the form

$$\langle|\boldsymbol{E}_D(\boldsymbol{R})|^2\rangle = \frac{2k^4p^2}{3R^2}\left[1+\sum_j \chi_j(\boldsymbol{k},\boldsymbol{r}_j)\right]. \tag{16}$$

Here

$$\chi_j(\boldsymbol{k},\boldsymbol{r}_j) = \int \rho_j(\boldsymbol{r}-\boldsymbol{r}_j)\chi_0(\boldsymbol{k},\boldsymbol{r})\,\mathrm{d}^3r \tag{17}$$

is the contribution of a single atom to the hologram and

$$\chi_0(\boldsymbol{k},\boldsymbol{r}) = -2r_e\,\mathrm{Re}\,\frac{\mathrm{e}^{\mathrm{i}(kr-\boldsymbol{k}\cdot\boldsymbol{r})}}{r}\left\{P_0(\theta)+[2-3P_0(\theta)]\left(\frac{1}{r^2k^2}-\frac{\mathrm{i}}{rk}\right)\right\} \tag{18}$$

is the hologram of an electron. The latter we can rewrite as

$$\chi_0(\boldsymbol{k},\boldsymbol{r}) = -2\frac{r_e}{r}\left[\left\{P_0(\theta) + [2-3P_0(\theta)]\frac{1}{k^2r^2}\right\}\cos(kr-\boldsymbol{k}\cdot\boldsymbol{r}) + [2-3P_0(\theta)]\frac{1}{rk}\sin(kr-\boldsymbol{k}\cdot\boldsymbol{r})\right]. \tag{19}$$

In the limit of $rk \gg 1$, $\chi_0(\boldsymbol{k},\boldsymbol{r})$ becomes

$$\chi_0(\boldsymbol{k},\boldsymbol{r}) \approx -2\frac{r_e}{r}P_0(\theta)\cos(kr-\boldsymbol{k}\cdot\boldsymbol{r}) \tag{20}$$

which is the usual expression of the hologram of an electron [14, 15]. For rk values near to one, the other two terms in equation (19) become important. As an example we take a NiO crystal. For this material, the nearest neighbour distance is $r = 2.09$ Å and the wavelength of the Ni Kα radiation is $\lambda = 1.66$ Å. This gives $1/rk = 0.13$ and $1/r^2k^2 = 0.016$. Since $P_0(\theta)$ varies between $\frac{1}{2}$ and 1, and $[2-3P_0(\theta)]$ is between -1 and $\frac{1}{2}$, in equation (19) the correction to the amplitude of the cosine function can be neglected, but the last term containing the sine function should be taken into account.

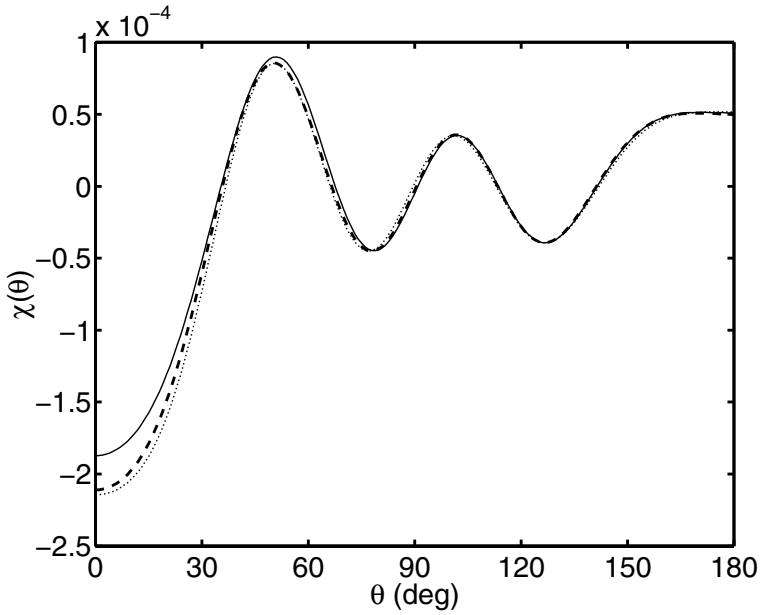

Figure 1. Calculated 'normal' hologram of a single oxygen atom at a distance of 2.09 Å from the fluorescent nickel atom as a function of the scattering angle θ. We used the wavelength of the Ni Kα radiation ($\lambda = 1.66$ Å). The dotted line is calculated using the usual far field approximations. The dashed line is based on expressions suggested by Adams and co-workers [8], which include some, but not all, near field effects. The solid line shows the result of the present calculation.

In figure 1 we compare the hologram of a single atom calculated in various approximations. For a single scatterer the hologram depends only on the scattering angle θ. The simplest approximation neglects all near field effects and the electron distribution of the atom is taken into account by replacing r_e in equation (20) by the plane wave atomic scattering length $f(\theta)$ (dotted line in figure 1). The next approximation is suggested by Adams and co-workers [8], and given by replacing r_e in equation (19) by $f(\theta)$ (dashed line). The third

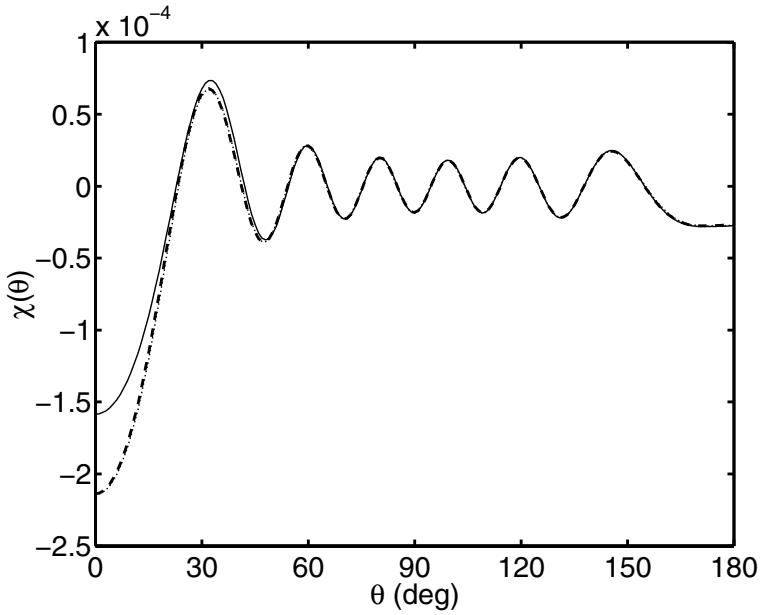

Figure 2. Same as figure 1 but with $\lambda = 0.69$ Å. The dotted and dashed lines nearly coincide.

(solid) line shows the result of the present calculation, based on equations (17) and (19). The integral in equation (17) is calculated numerically. The largest difference between the present and previous calculations appears near to the forward scattering direction. We note here that with increasing r all curves approach the far field limit. Similar behaviour can be observed with increasing k for the near field approximations represented by the dashed curve (figure 2). However, our calculations (solid line) show that in the forward scattering region the scattering amplitude becomes even smaller. This is due to the increasing phase shifts as the wavelength becomes smaller relative to the path length differences inside the atomic electron cloud.

Now we turn to the inverse x-ray fluorescent holography. In this case the sample is irradiated by x-rays from a well defined direction. The superposition of this and the scattered beam may excite an atom, which subsequently emits fluorescent radiation. The total yield of this fluorescent radiation is measured as a function of the direction of the incident beam. 'Inverse' x-ray holography experiments are usually done with linearly polarized synchrotron radiation. Figure 3 shows schematically two possible experimental set-ups. In figure 3(a) the ϑ-axis of the sample movement is perpendicular to the polarization vector of the synchrotron radiation, while in figure 3(b) it is parallel. Both arrangements have been used in the past [4, 16–23].

The amplitude of the incident x-radiation is written in the form of a plane wave:

$$\boldsymbol{E}(\boldsymbol{r}) = \boldsymbol{E}_p \, \mathrm{e}^{-\mathrm{i}\boldsymbol{k}\cdot\boldsymbol{r}}. \tag{21}$$

The vector $\boldsymbol{E}_p$ defines the polarization of the plane wave. This radiation scatters on the electrons in the sample before absorbed by the 'detector' atom at the origin. The incoming plane wave induces a dipole moment on an electron placed at $\boldsymbol{r}$:

$$\boldsymbol{p} = -\frac{r_e}{k^2}\boldsymbol{E}_p \, \mathrm{e}^{-\mathrm{i}\boldsymbol{k}\cdot\boldsymbol{r}}. \tag{22}$$

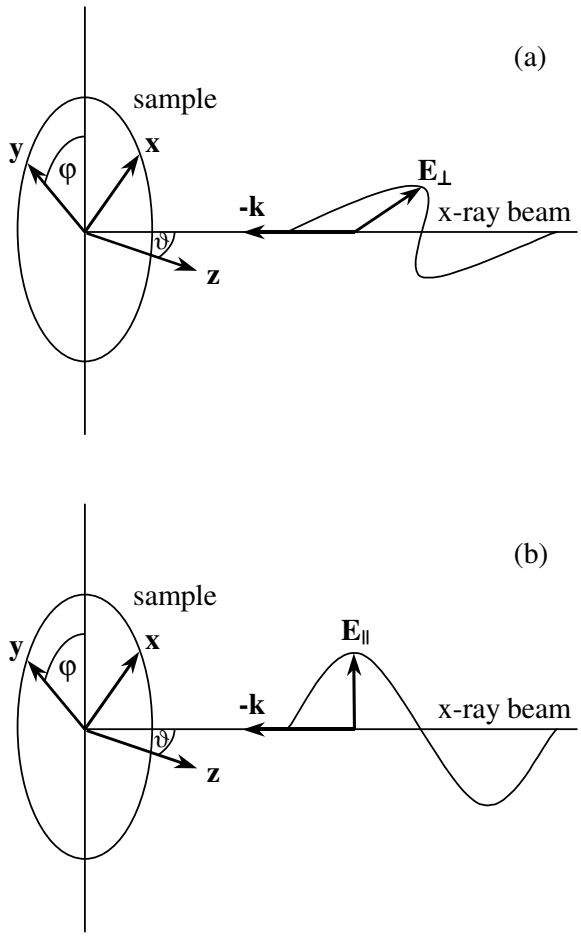

Figure 3. Sketch of the two usual experimental set-ups for 'inverse' x-ray holography. The ϑ-axis of the sample movement (vertical line) can be perpendicular (a) or parallel (b) to the polarization plane of the incident x-ray beam. The vectors $\boldsymbol{x}$ and $\boldsymbol{y}$ are in the plane of the sample while $\boldsymbol{z}$ is perpendicular to it. Together they form a coordinate system fixed to the sample.

The amplitude of the wave at the origin scattered by an electron at $\boldsymbol{r}$ is given by inserting this dipole moment into equation (1):

$$\boldsymbol{E}_0(\boldsymbol{r},\boldsymbol{k}) = -r_e\left\{(\boldsymbol{n}'\times\boldsymbol{E}_p\times\boldsymbol{n}') + [3\boldsymbol{n}'(\boldsymbol{n}'\cdot\boldsymbol{E}_p) - \boldsymbol{E}_p]\left(\frac{1}{r^2k^2} - \frac{\mathrm{i}}{rk}\right)\right\}\frac{\mathrm{e}^{\mathrm{i}(kr-\boldsymbol{k}\cdot\boldsymbol{r})}}{r}. \tag{23}$$

The electric field at the detector atom has two contributions: the incident plane wave and the wave scattered by the electron distribution in the solid:

$$\boldsymbol{E}_D(\boldsymbol{k}) = \boldsymbol{E}(0) + \int \rho(\boldsymbol{r})\boldsymbol{E}_0(\boldsymbol{r},\boldsymbol{k})\,\mathrm{d}^3r. \tag{24}$$

Inserting equations (6), (21) and (23) leads to

$$\boldsymbol{E}_D(\boldsymbol{k}) = \boldsymbol{E}_p - r_e\sum_j\int \rho_j(\boldsymbol{r}-\boldsymbol{r}_j)$$
$$\times\left\{(\boldsymbol{n}'\times\boldsymbol{E}_p\times\boldsymbol{n}') + [3\boldsymbol{n}'(\boldsymbol{n}'\cdot\boldsymbol{E}_p) - \boldsymbol{E}_p]\left(\frac{1}{r^2k^2} - \frac{\mathrm{i}}{rk}\right)\right\}\frac{\mathrm{e}^{\mathrm{i}(kr-\boldsymbol{k}\cdot\boldsymbol{r})}}{r}\,\mathrm{d}^3r. \tag{25}$$

The total fluorescent yield of the 'detector' atom is proportional to the intensity at the origin. Similar to the 'normal' holography, we can neglect the term proportional to r_e^2:

$$|\boldsymbol{E}_D(\boldsymbol{k})|^2 \approx E_p^2 - 2r_e \,\mathrm{Re} \sum_j \int \rho_j(\boldsymbol{r}-\boldsymbol{r}_j)\boldsymbol{E}_p \times\left\{(\boldsymbol{n}'\times\boldsymbol{E}_p\times\boldsymbol{n}')+[3\boldsymbol{n}'(\boldsymbol{n}'\cdot\boldsymbol{E}_p)-\boldsymbol{E}_p]\left(\frac{1}{r^2k^2}-\frac{\mathrm{i}}{rk}\right)\right\}\frac{\mathrm{e}^{\mathrm{i}(kr-\boldsymbol{k}\cdot\boldsymbol{r})}}{r}\,\mathrm{d}^3r. \quad (26)$$

Expressing again the vector product in terms of scalar products and introducing the polarization factor

$$P_p = 1 - \frac{(\boldsymbol{E}_p\cdot\boldsymbol{n}')^2}{E_p^2} = 1 - \frac{(\boldsymbol{E}_p\cdot\boldsymbol{r})^2}{E_p^2 r^2} \quad (27)$$

the intensity can be written in the form

$$|\boldsymbol{E}_D(\boldsymbol{k})|^2 = E_p^2\left[1+\sum_j \chi_k^p(\boldsymbol{k},\boldsymbol{r}_j)\right]. \quad (28)$$

Here

$$\chi_j^p(\boldsymbol{k},\boldsymbol{r}_j) = \int \rho_j(\boldsymbol{r}-\boldsymbol{r}_j)\chi_0^p(\boldsymbol{k},\boldsymbol{r})\,\mathrm{d}^3r \quad (29)$$

and

$$\chi_0^p(\boldsymbol{k},\boldsymbol{r}) = -2\frac{r_e}{r}\left[\left\{P_p+[2-3P_p]\frac{1}{r^2k^2}\right\}\cos(kr-\boldsymbol{k}\cdot\boldsymbol{r})+[2-3P_p]\frac{1}{rk}\sin(kr-\boldsymbol{k}\cdot\boldsymbol{r})\right]. \quad (30)$$

Not regarding the scaling factor, equations (28)–(30) differ from equations (16)–(19) only in the polarization factor P_p. In the case of an unpolarized incident beam we average equation (27) for the direction of $\boldsymbol{E}_p$ while keeping it perpendicular to $\boldsymbol{k}$:

$$P_0 = 1 - \frac{\langle(\boldsymbol{E}_p\cdot\boldsymbol{r})^2\rangle}{E_p^2 r^2} = \frac{1+\cos^2\theta}{2}. \quad (31)$$

Except the scaling factors, we obtained the same expressions for 'inverse' holography with an unpolarized beam as for 'normal' holography. The only important difference between the two cases is that while in 'normal' holography the fluorescent radiation forms the hologram, in 'inverse' holography it is done by the incident beam.

While 'inverse' x-ray holography can be done with unpolarized radiation [19], in most cases linearly polarized synchrotron radiation is used. When the polarization vector $\boldsymbol{E}_p$ is perpendicular to the ϑ-axis of the sample movement (see figure 3(a)), the polarization factor is

$$P_\perp = 1 - \frac{(\boldsymbol{E}_\perp\cdot\boldsymbol{r})^2}{E_\perp^2 r^2} = 1 - (x\cos\vartheta\cos\varphi + y\cos\vartheta\sin\varphi - z\sin\vartheta)^2/r^2 \quad (32)$$

where x, y, z are components of vector $\boldsymbol{r}$ and we expressed the wavevector $\boldsymbol{k}$ in spherical coordinates ϑ and φ defined in figure 3. Note that θ and ϑ are identical only if the scattering atom is on the z-axis. In figure 4 we compare our results for the case of perpendicular polarization with the same two approximations as we did for the unpolarized case. Again, the largest deviations can be observed near to forward scattering. At $\vartheta = 90^\circ$, neglecting the near field effects (dotted line) leads to vanishing holographic signal as $\boldsymbol{r}$ and $\boldsymbol{E}_\perp$ are parallel. The more accurate calculations (dashed and solid lines) show that there is always

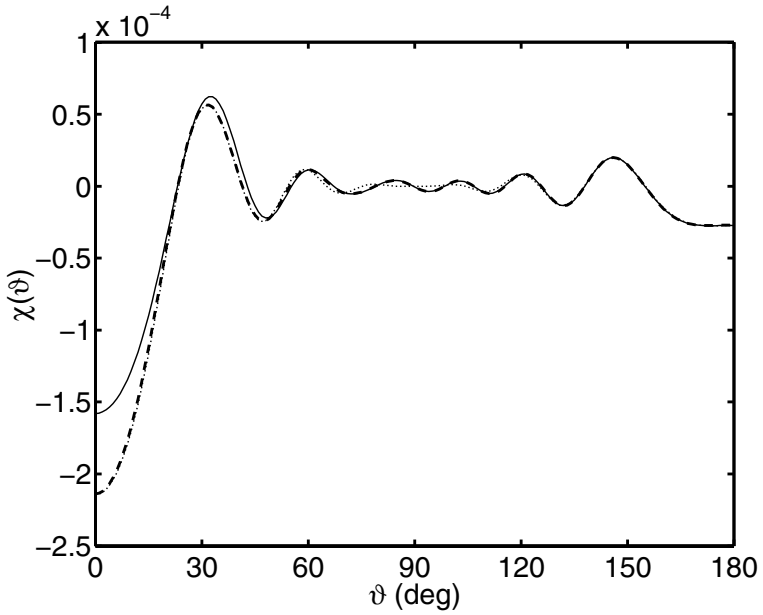

Figure 4. Same as figure 2 but for 'inverse' x-ray holography with perpendicular polarization (figure 3(a)). The oxygen atom is on the z-axis.

a non-vanishing contribution from that part of the electron cloud which does not satisfy this condition.

In the other usual arrangement, when the polarization vector $\boldsymbol{E}_p$ is parallel to the ϑ-axis (figure 3(b)) P_p becomes

$$P_{\parallel} = 1 - \frac{(\boldsymbol{E}_{\parallel} \cdot \boldsymbol{r})^2}{E_{\parallel}^2 r^2} = 1 - (x \sin\varphi - y \cos\varphi)^2 / r^2. \tag{33}$$

In this case the polarization factor is independent of angle ϑ.

3. Comparison of calculated and measured hologram

The measured hologram contains contributions of a large number of atoms. The frequency of the oscillations is roughly proportional to the distance of the scattering atom. It was pointed out earlier [14] that applying a low pass filter removes the Kossel lines (or x-ray standing wave lines in the 'inverse' case) while it keeps the contributions of atoms near to the source (or detector) atom. Nevertheless, far atoms may also give some contribution to the low frequency part of the hologram. Therefore, we have to take into account a relatively large number of atoms, if we want to compare the results of the calculations to real measurements. The near field effects originating from the curvature of the wavefront decrease rapidly with increasing distance. Since the three-dimensional integration in equation (29) requires a large amount of computing power, we take into account these effects only for the first few coordination shells.

We have chosen nickel oxide as model material, since good quality holograms were recorded earlier on a single crystalline NiO sample [20]. The measurements were made at the European Synchrotron Radiation Facility in the 'inverse' mode with the ϑ-axis perpendicular

to the polarization of the x-ray beam (figure 3(a)). The Ni Kα fluorescent line was used to detect the hologram.

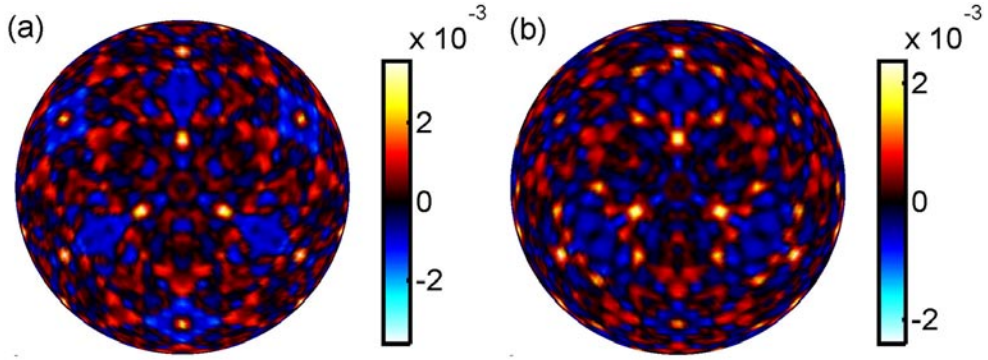

Figure 5. Calculated (a) and measured (b) x-ray holograms of NiO at $\lambda = 0.69$ Å. In the calculation about 33 000 atoms were taken into account. The hologram of a NiO single crystal was measured in the 'inverse' mode at the European Synchrotron Radiation Facility [20].

We have calculated the hologram of a spherical NiO cluster containing more than 33 000 atoms. The x-ray wavelength used ($\lambda = 0.69$ Å, $E = 17.9$ keV) was the same as one of the wavelengths of the measurement [20]. The curvature of the wavefront was taken into account for the 32 atoms (18 Ni and 14 O) nearest to the central Ni atom. On the results of the calculation we applied the same low pass filter as on the experimental data. We compare the results in figure 5. It can be seen that although not all details are exactly the same, the main features of the measured and calculated holograms agree very well. The small differences can be explained by the limited size of the cluster used in the calculation.

4. Conclusion

It is clear from the above discussion that theory and experiment develops in parallel. So the formation of x-ray holograms is well understood. However, this does not mean that precise 3D atomic order can be easily obtained from the measured data. Why? Because we do not want to lose the simplicity of the traditional holographic reconstruction. The use of the Helmholtz–Kirchhoff integral transformation gives directly a 3D picture without any assumption. However, this type of evaluation does not take into account the distortions discussed in this paper. Therefore atomic positions and the brightness of atoms (which is proportional to the number of electrons) might be in error after simple Helmholtz–Kirchhoff transformation. However, the fact that we can calculate holograms very precisely gives the basis for iterative algorithms. In this type of evaluation one could take into account polarization effects and the distortion caused by the curvature of the wavefront.

Finally a few words about experimental techniques. Methods for performing normal and inverse x-ray fluorescent holographic experiments are refined. High quality data can be routinely taken. Of course the speed of accumulating holograms might be increased; parts of the experimental setup can be improved. However, the real bottleneck on the experimental side is the form of the sample (presently a large flat single crystal) which we are able to measure. Clearly more work is needed in the direction of small arbitrary shaped samples. Another side of the experimental technique is non-fluorescent experiments. Many interesting possibilities are open. There was one experiment using bremsstrahlung radiation [24] and another one using

gamma photons from nuclear decay [25] to form holograms. Both need much more work to bring them from the demonstration stage to application. Beside photons, other particles such as neutrons might be used for holographic imaging. Holography with neutrons seems very difficult, because of the small scattering cross section of these particles. However, in special cases when we select isotopes with relatively large scattering cross section and others with large absorption cross section, and we combine these in one sample, there is some chance to see a hologram.

Concluding we can tell that the formation of holograms in fluorescent x-ray holography is well understood, but the field of atomic resolution holography in general is full of open questions. We hope that outlining some of the problems and possibilities induces the concentration of effort in these directions.

Acknowledgments

This work was supported by OKTA T034284 and the EU Centre of Excellence Programme.

References

[1] Saldin D K and de Andres P L 1990 *Phys. Rev. Lett.* **64** 1270
[2] Harp G R, Saldin D K and Tonner B P 1990 *Phys. Rev. Lett.* **65** 1012
[3] Tegze M and Faigel G 1996 *Nature* **380** 49
[4] Gog T, Len P M, Materlik G, Bahr D, Fadley C S and Sanchez-Hanke C 1996 *Phys. Rev. Lett.* **76** 3132
[5] We list here only a few of the numerous papers: Barton J J 1991 *Phys. Rev. Lett.* **67** 3106
Tonner B P, Han Z-L, Harp G R and Saldin D K 1991 *Phys. Rev.* B **43** 14 423
Tong S Y, Li H and Huang H 1995 *Phys. Rev.* B **51** 1850
Tong S Y 1999 *Adv. Phys.* **48** 135
Wider J *et al* 2001 *Phys. Rev. Lett.* **86** 2337
[6] Barton J J 1988 *Phys. Rev. Lett.* **61** 1356
[7] Len P M, Gog T, Novikov D, Eisenhower R A, Materlik G and Fadley C S 1997 *Phys. Rev.* B **56** 1529
[8] Adams B, Novikov D V, Hiort T, Materlik G and Kossel E 1998 *Phys. Rev.* B **57** 7526
[9] Miller G A and Sorensen L B 1997 *Phys. Rev.* B **56** 2399
[10] Nishino Y and Materlik G 1999 *Phys. Rev.* B **60** 15 074
[11] Szöke A 1986 *Short Wavelength Coherent Radiation: Generation and Applications (AIP Conf. Proc. 147)* ed D T Attwood and J Boker (New York: American Institute of Physics) p 361
[12] Jackson J D 1975 *Classical Electrodynamics* (New York: Wiley)
[13] Kossel W, Loeck V and Voges H 1935 *Z. Phys.* **94** 139
[14] Tegze M and Faigel G 1991 *Europhys. Lett.* **16** 41
[15] Faigel G and Tegze M 1999 *Rep. Prog. Phys.* **62** 355
[16] Novikov D V, Adams B, Hiort T, Kossel E, Materlik G, Menk R and Walenta A 1998 *J. Synchrotron Radiat.* **5** 315
[17] Kawai J, Hayashi K, Yamamoto T, Hayakawa S and Gohshi Y 1998 *Anal. Sci.* **14** 903
[18] Hayashi K, Yamamoto T, Kawai J, Suzuki M, Goto S, Hayakawa S, Sakurai K and Gohshi Y 1998 *Anal. Sci.* **14** 987
[19] Tegze M, Faigel G, Marchesini S, Belakhovsky M and Chumakov A I 1999 *Phys. Rev. Lett.* **82** 4847
[20] Tegze M, Faigel G, Marchesini S, Belakhovsky M and Ulrich O 2000 *Nature* **407** 38
[21] Marchesini S, Schmithüsen F, Tegze M, Faigel G, Calvayrac Y, Belakhovsky M, Chevrier J and Simionovici A 2000 *Phys. Rev. Lett.* **85** 4723
[22] Marchesini S, Ulrich O, Faigel G, Tegze M, Belakhovsky M and Simionovici A S 2001 *Nucl. Instrum. Methods* A **457** 601
[23] Hayashi K, Matsui M, Awakura Y, Kaneyoshi Y, Tanida H and Ishii M 2001 *Phys. Rev.* B **63** 041201(R)
[24] Bompadre S G, Petersen T W and Sorensen L B 1999 *Phys. Rev. Lett.* **83** 2741
[25] Korecki P, Korecki J and Slezak T 1997 *Phys. Rev. Lett.* **79** 3518